Springer

KSME

Journal of Mechanical Science and Technology 33 (6) (2019) 2651~2663
www.springerlink.com/content/1738-494x(Print)/1976-3824(Online)
DOI 10.1007/s12206-019-0513-9

Investigation of shedding patterns and its influences on lift performances of a cylinder bundle in cross flow †

Di Tang[1], Shiyi Bao[1,*], Binbin Lv[2], Hao Cui[3], Lijia Luo[1] and Min Xu[4]

[1]*College of Mechanical Engineering, Zhejiang University of Technology, Hangzhou 310014, China*
[2]*High Speed Aerodynamic Institute, China Aerodynamics Research and Development Center, Mianyang 621000, China*
[3]*Shenyang Aircraft Design and Research Institute of AVIC, Shenyang 110035, China*
[4]*New Mexico State University, Las Cruces, NM, 88001, USA*

(Manuscript Received July 31, 2018; Revised December 28, 2018; Accepted March 13, 2019)

Abstract

Shedding vortices in cross flow are of much practical importance in the analysis of flow induced vibrations of a steam generator. However, studies of shedding vortex are still few in present, especially in shedding patterns and its influences on lift performances. In this paper, five basic shedding patterns were investigated by numerical simulations of a 2D unsteady flow around a bundle with 253 cylinders. The numerical results clearly demonstrated that *flow in line* is the most common pattern. On the hand, the other four shedding patterns, *cross in line*, *cross near line near*, *cross near line far* and *cross far line near*, appear randomly. Influences of shedding vortices on lift performances were concluded as *lift enhancement*, *lift pit* and *lift lag*. These numerical results can provide a basic knowledge of shedding vortices for cylinders and can precisely quantify their influences on unsteady lift performances.

Keywords: Shedding vortices; Lift performances; Cross flow; Heat exchanger tube; Nuclear

1. Introduction

The pressures on global warming issues are attracting the international attentions, reductions of carbon dioxide (CO_2) emission have envisaged in worldwide [1]. On the other hand, demands for energy of the world are continuously rising, it is reported that an increase of 50 % from 2016 to 2030 will be expected from the International Energy Agency [2, 3]. Thus, confronting the double pressures of the environment destruction and the energy demands, nuclear energy is playing an important role. For instance, Switzerland, as an interconnecting hub linking three biggest European national markets of Germany-Austria, France and Italy, 38 % of the electricity generation comes from nuclear in 2014 [4]. As French, even 76 % of the electricity generation comes from nuclear [5]. China, as one of the largest developing countries, has proposed the medium and long term nuclear energy development plan (2005-2020) to promote the production capacity of nuclear power [6]. However, since the Fukushima nuclear accident, each country is more cautious about vulnerability of nuclear energy and try to reduce all the risks in nuclear power plant [7]. Among kinds of risks, the vibrations of pipes threat the reliability of power system which is one of the major aspects in the energy security narratives.

Until now, many works have been done to investigate vibrations or flow-induced vibrations of heat exchanger tubes [8], in which unsteady fluid forces and U-bend structural modelling are the two most important components [9]. Due to the complexity of unsteady flow, much efforts have been made to predict the vibrational forces or reveal flow phenomena. As a single circular cylinder, Coutanceau and Defaye [10] did a detailed survey of flow visualization of cross flow. And influences on the cross flow over a cylinder had been experimentally investigated [11], it was shown that the regular vortex shedding was suppressed when the dimensionless gaps between wall and a cylinder are less than 0.3, on the hand, the Strouhal number kept constant when the gaps are greater than 0.3. Recently, drag forces, lift forces, shedding vortices, as well as interactions with a wall of a single cylinder are further investigated which can be found in the works of Buresti, Lanciotti, Nishino [12, 13]. In comparison to a fixed one, vortex shedding has been experimentally found to be affected by cylinder vibration of a spring supported wide-D-section cylinder [14], a 2P (two pair) vortex mode exists in the wake rather than S mode (single vortex) [15], the velocity deficit behind the cylinder and the mean drag coefficient are much larger.

In fact, wake interactions of a heat exchanger may be too complex due to the large number of tubes, the simplest case to

*Corresponding author. Tel.: +86 571 88871068, Fax.: +86 571 88871068
E-mail address: bsy@zjut.edu.cn; tangdi@zjut.edu.cn
† Recommended by Associate Editor Hyoung-gwon Choi

study the unsteady flow with multiple cylinders is two cylinders in tandem or stagger arrangement. It has been reported that flow structures are quite sensible to the gap between two cylinders where shedding vortices separate. Flow and flow induced vortices shed from two cylinders both in tandem and stagger arrangement were studied with experimental method [16, 17], the corresponding flow can be classified as three regimes according to the space ratio L/D, which are extended-body regime, reattachment regime and co-shedding regime [18]. A two-cylinder case was studied in a water tunnel in which the upstream cylinder was fixed while the downstream cylinder could vibrate freely [19], the wake Galloping phenomenon also was found and researched in this study. Whereas the tube number of a heat exchanger in a nuclear plant is usually large, the cross flow over a tube bundle need to be investigated in detail [20, 21]. Early works about tube bundle were done at 1981, Weavera and Elkashlana [22] investigated the cross flow induced vibrations in tube banks and recommended six rows should be used. Since then, several rows of cylinders were usually used for the cross-flow research, for instance, Zukauskas and Ulinskas recommended 4 rows for heat transfer [21]. Duan and Jiang [23] used 5 rows of tubes to simulate the flow distribution of a 3D helical tube bundle with RANS method. Beatriz de Pedro [24] recently used a commercial CFD code to simulate the unsteady flow of normal triangular cylinder with one single tube undergoing oscillations based on 2D URANS methods. Abramov [25] simulated the turbulent flow and heat transfer in cross flow over inline tube bundles based on the SST turbulence model. In the study, a series of cylinder cases, with a maximum column number of 10 and a maximum row number of 7 were studied. It was found that an acceptable level of agreement was achieved when three or more tube rows were included in the cross direction by comparing the computed and the experimental data.

When steam or water flow across a heat exchanger, a typical cross flow is formed, and an adverse pressure gradient is raised up followed by separations in shear layer of a tube. Thus, some small-scale vortices are generated in the corresponding shear flow, those vortices are coalescing with each other [26] resulting in stronger vortices, and finally a pair of co-rotating line vortices will be generated [27]. The line vortices shed from the tube in turns, however, if there is no tubes or other solid bodies in the wake region, the line vortices will give rise to Karman vortex shedding and heat exchanger tubes will suffer from strong cross forces. Thus, unsteady loads of a cylinder will be significantly affected by those shedding vortices and the wake of each tube is considered to be very critical, therefore, Roshko [28, 29], Gerrard [30] studied the vortex and wake formation of a cylinder, Grove et al. [31] investigated the steady separated flow passing a cylinder at a low Re ranging from 25 to177. As the cylinder bundles, Ormiston et al. [32] investigated turbulent fluid flows across staggered tubes using both numerical and experimental methods, and a higher transverse turbulent intensity was predicted. Thole et al. [33] studied the wake development of a staggered tube bank using PIV method at Re ranging from 3000 to 20000. It was reported that the Strouhal number and fluctuation in the velocity increased against decrease of stream wise spacing. Chidan- and Mangrulkar [34] studied cross flow of a tube bank in staggered arrangements with a splitter plate attachment using both experimental and numerical method, it was reported that the overall thermal performance of splitter attachment is superior to the bare one.

In the aspect of numerical method, a lot of methods have been contributed to understand flow characteristics [35], flow loads are commonly predicted by engineering approximation methods based on the main features of Karman vortex, such as the standards GB151, TEMA et al. [36, 37]. The critical speed, drag coefficients and lift coefficients are usually calculated by speed of cross flow. As the development of computational fluid dynamics (CFD), the N-S equations now are computed to predict the unsteady flow loads. Reynolds-averaged Navier-Stokes (RANS) method, detached eddy simulation (DES), and large eddy simulation (LES) are the three main methods. The SST turbulent model of RANS is a commonly used model in cross flow around circular cylinders [25, 38]. The modified SST turbulent with transition model to some extent improves the simulation accuracy especially in predictions of transition and separation. However, the eddy viscosity will be overestimated and some important vortex structures will be expunged in unsteady flow using the RANS method. Unfortunately, the unsteady vortices are the major characteristics in flow with tubes. The overcome the previously problem, some filters have been introduced to improve the simulation precision in LES method. But the huge amount of computation has greatly limited its application in engineering of heat exchanger tubes. Compromising on numerical precision and computational amount, the DES method is developed by combining RANS and LES methods [39, 40]. It's worth mentioning that the direct numerical simulation (DNS) method has also been used in crossflow simulations in recent years [41, 42]. However, the computational amount is quite huge which has greatly limited its application in 3D simulation of heat exchanger tubes.

As mentioned, much work has been devoted to identify the unsteady loads or instability, however, little work has been achieved in the domain of shedding vortices due to cross flow [43]. But explaining and understanding the unsteady onset such as the shedding vortices are of paramount importance concerning fundamental phenomena in the domain of unsteady performances [44]. Thus, the main objective of present research is the further understanding of the vortex's characteristics of cross flow with hundreds of tubes as well as the corresponding influences on the lift performances. Reliable and comprehensive vortices data are obtained and the mechanism of the influences on the lift performances are revealed. This numerical simulation research program includes (a) description of CFD method and modeling method of tube bundles in Sec. 2, (b) numerical simulation of a single cylinder to verify the CFD method in Sec. 3.1, (c) the vortex characteristics of

cylinders are discussed in Sec. 3.2, (d) the influences of shedding vortices on the lift performances are discussed in Sec. 3.3.

2. Numerical and modeling method

2.1 CFD method

The governing equations are impressible Navier-Stokes equations which were solved using the Fluent software (of Fluent Inc., USA). SIMPLEC algorithm was used for pressure and velocity coupling. Pressure based solver was chosen with explicit formulation. Space discretization scheme of pressure equation used second order, discretization scheme of momentum used QUICK scheme. A small time-step of 3×10^{-5} was used, which was estimate by the characteristic of shedding vortices. The continuity equations are:

$$\nabla \cdot V = 0 . \tag{1}$$

The momentum equations are:

$$\rho[\frac{\partial V}{\partial t} + V \cdot \nabla V] = -\nabla p + \mu \nabla^2 V \tag{2}$$

where t is the time, V is the velocity, p is the pressure, μ is the coefficient of dynamic viscosity.

The flow before the tube bundle is usually the laminar flow, while the flow in the gaps is mainly turbulent flow. The Transition SST model which is more accurate and adaptive for such situation has been applied to the vapor [45]. The $\gamma-\theta$ Gamma-Theta transition model has been used, the further details of the SST model and the transport equation can be found in ANSYS manual [46].

2.2 Physical modeling

In this study, we follow configuration of tube arrays discussed in Ref. [47], where flow-induced vibration of nuclear steam generator U-tubes was studied by experiment approach. 2D model can represent vortex shedding in some particular conditions due to the similarities in vortex shedding, as discussed in Ref. [22], thus a cut plane was placed in the middle plane as shown in Fig. 1. A 2D model with 253 cylinders is obtained and used to study the flow dynamics as well as vortex shedding features. Diameter of each tube is 19.05 mm. The vertical region has a triangular array with a pitch of 25.4 mm. The horizontal region of the U-tubes has a rotated square array with a pitch of 31.11 mm, which gives a pitch over diameter ratio, P/d = 1.633. The experimental model and the simplified sketch on the cut plane at the middle section are depicted in Fig. 1.

2.3 Definitions

Lift force is the main factor that excites vibrations of a tube. The lift coefficient (C_L) is normalized with the upstream undisturbed flow velocity V, cylinder diameter D, vapor density ρ and lift force L

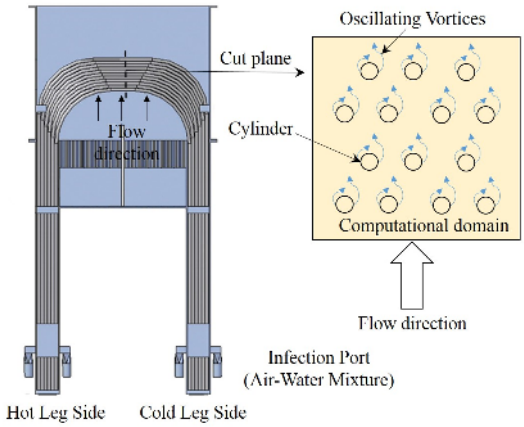

Fig. 1. Physical modeling of the U-tubes [45].

$$C_L = \frac{L}{\frac{1}{2}\rho V^2 D} . \tag{3}$$

The vorticity in z direction is defined as follows

$$\omega_z = \frac{\partial V_y}{\partial x} - \frac{\partial V_x}{\partial y} . \tag{4}$$

2.4 Numerical example of a single cylinder

To verify the numerical method of this paper, a benchmark is studied. A good prediction of pressure gradient, liquid hold up, shedding vortices, et al, of pipes is essential for flow simulations [48]. Therefore, various flow patterns have been developed, such as stratified flow, slug flow, annular flow and dispersed flow. Each patter is suitable for different fluid properties or flow condition, and the RANS method is adopted to simulate the unsteady flow in this paper. In this section, to verify the solver of CFD, a case of flow around a circular cylinder is studied, after then the CFD method is used to simulate the flow with hundreds of cylinders. The numerical experiences were arranged based on the experiments of $Re = 2.6\times10^5$ in Ref. [49]. The reference length scale was 150 mm, the total height of the roughness was 2 μm , and the fluid was air. A structural computational domain of $60D\times 90D60D\times180D$ is adopted by discretizing the flow region with 63 thousand nodes, as shown in Fig. 2. In the x-y plane, the cylinder is discretized uniformly with 181 nodes. The radial size of the first layer is set according to a non-dimensional wall distance y^+ less than 1 for the Reynolds number $Re = 2.6\times10^5$. The cell expansion ration in the whole domain is kept below 1.1. For the snake of capturing wake structures, a higher mesh resolution in the near wake is used.

Fig. 3 compares distribution of time-averaged pressure coefficient (Cp) on the cylinder surface, obtained from current

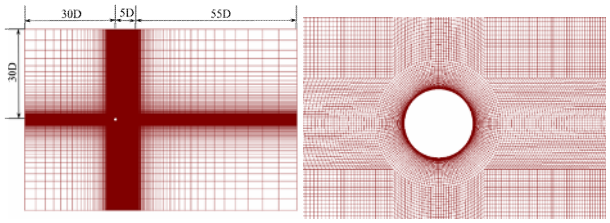

Fig. 2. Computational domain and the close-up view.

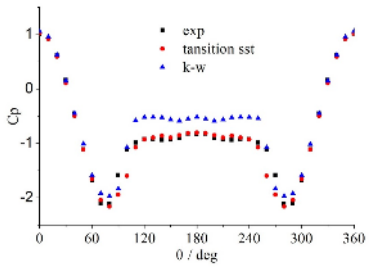

Fig. 3. Distribution of Cp on the cylinder surface.

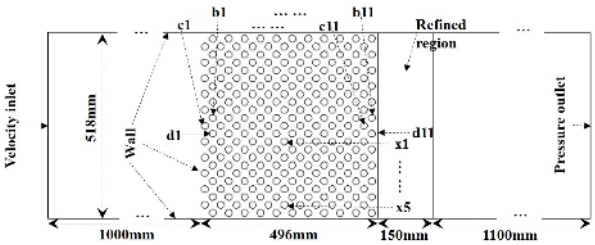

(a) Global overview

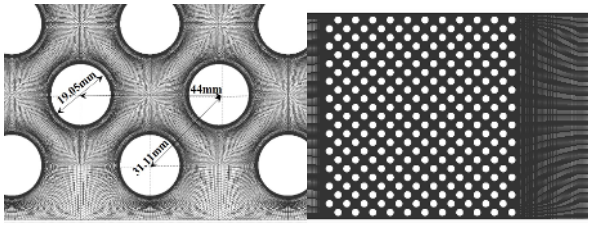

(b) Overview of cylinders (b) Local view of cylinders

Fig. 4. Grid and computational domain of the cylinder bundle.

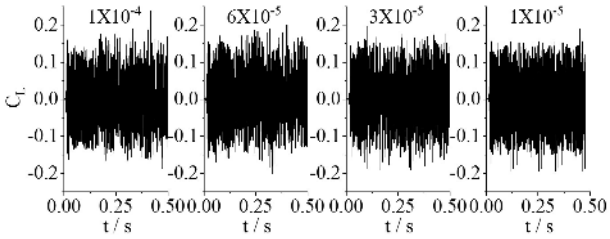

Fig. 5. Independence analysis of time step.

numerical simulation and the experiment measurements by Achenbach [49]. Both the result of $k-\omega$ model and the one of SST model agree well with the experimental data before 120°. However, large deviations are observed for the $k-\omega$ model between 120° and 240°, thus the SST model is used in this paper. The Cp achieves a maximum value of 1.0, which matches the theoretical value, and reaches a minimum value of -2.16, which fits well with the experimental value of -2.11. Despite of a small deviation between 80° and 120°, where flow separation occurs, the computational results agree very well with the experimental data. Thus, the numerical method of this paper was verified.

3. Shedding vortices of cylinders

To simulate the innermost region of an actual steam generator, 253 cylinders is used in this paper which are arranged into 22 columns and 23 rows, O-blocks are used to construct mesh of the cylinder bundle with 2.35 million nodes according settings of the single cylinder in Sec. 3.1. For the snake of capturing wake structures, a fined grid is arranged behind the cylinder bundle with 5D length. A series of cylinders are marked as b1~b11, c1~c11, d1~d11, x1~x4 for the reference, illustrated in Fig. 4. The saturated steam flow passes the cylinder bundle through the inlet boundary at the left side with a uniform velocity of 7.4 m/s. The density of the steam is specified as 0.58 kg/m^3, while the dynamic viscosity is 1.22×10^{-5}. A pressure outlet with a reference value of zero is specified on the outlet at the right side. No-slip wall boundary conditions are specified on the top and bottom boundaries as well as the cylinder surfaces [50], as shown in Fig. 4(a). A typical Reynold number with 2.9×10^4 is obtained for a single cylinder.

Since the accuracy of numerical simulation is affected by the time step. Thus, different step sizes were used to find out a compromise between computational coasts and accuracy. The independence was conducted in the flow domain, with 1×10^{-4}, 6×10^{-5}, 3×10^{-5} and 1×10^{-5}. The lift coefficients were obtained in the 2D simulation for the four cases were detailed in Fig. 5. It can be seen that once the time step is small than 6×10^{-5}, all current results are close to previous simulations with a maximum 0.2 C_L, as shown in Fig. 5. Synthesizes the computational costs and accuracy, a time step with 3×10^{-5} were adopted.

Vortex intensity is determined using Eq. (6) and calculated shedding vortices in the flow region are shown in Fig. 6 with a contour legend range from -2000 to 2000. Both the clockwise and the anti-clockwise vortices are represented by blue and red colors respectively. For convenience and vividness, contour legends of the following vortex figures are all the same with the one of Fig. 6, and the corresponding vortex is called a red one or a blue one. The generated vortices and shedding processes are clearly visible in the flow domain. It is shown that a red vortex is generated in the shear layer above a cylinder, and a blue vortex is generated in the shear layer below a cylinder. A red vortex and a blue vortex may pair up with each other to form a jet flow between neighboring cylinders due to the staggered arrangement. However, there are no two identical vortices in the whole flow domain. It is implied that statistics and randomness are the two main characteristics of the vortex shedding which will be detailed in the following sec-

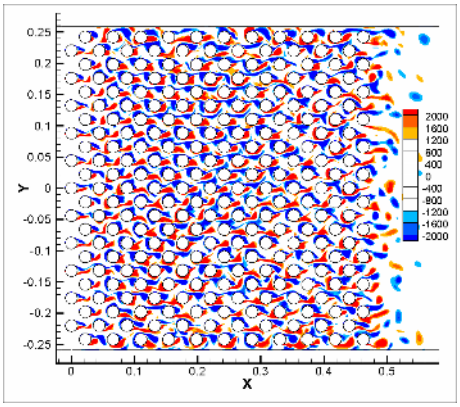

Fig. 6. Shedding vortices in the computational domain at time 0.614 s.

tions. On the other hand, the Strouhal number is a measure of the relevance of the aerodynamic effects in the flow, here the Strouhal number, 0.205, is calculated according the assumptions of Ref. [51].

3.1 Flow characteristics of c1 and c11

Vortices are generated from cylinders at the first row and finally shed from those of the last row with different shedding features. A deeper insight into vortices around c1 and d11 shows that one small blue vortex is developed in the shear layer upper the cylinder c1 followed by a small red vortex in the shear layer below c1, as depicted in Fig. 7(a). Till the completion of an oscillation period, a blue vortex and a red one are shed alternatively from both sides of c1. Before reach the cylinder c2, those vortices are split followed by change of flow directions. At the same time, new shedding vortices are generated around c2. As a split vortex has reached shear layer around a cylinder from upstream, the split vortex and new generated vortices will coalesce with each other to form some stronger vortices. Henceforth, each cylinder suffers from those upstream vortices and induces new vortices downstream. As a result, flow between c1 and c2 is greatly influenced by cylinder c1, b1 and d1, on the contrary, flow before c1 is less influenced because c1 is ahead of the cylinder bundle.

Both stream lines and shedding vortices are forced to the center line of c1 as shown in Fig. 7(a). Lag of vortex separation of c1 indicates that an adverse pressure gradient around c1 is delayed. Generally, separation of a single cylinder begins at 90º [52], however, vortex separation of c1 is put off till 103º. On the one hand, strength and flow direction of the shedding vortex are changed dramatically, all the shedding vortices of c1 are confined to a small triangular region as shown in Fig. 7(a). On the contrary to the flow characteristics of c1, blue vortices in the shear layer of d11 shed nearly at 90º which is replicated by the red vortex shedding. This may due to the combined action of shedding vortices ahead of d11 and no cylinders downstream. As a result, there is a relatively stable region behind d11 which is named as ‘dead zone’ shown in Fig. 7(c).

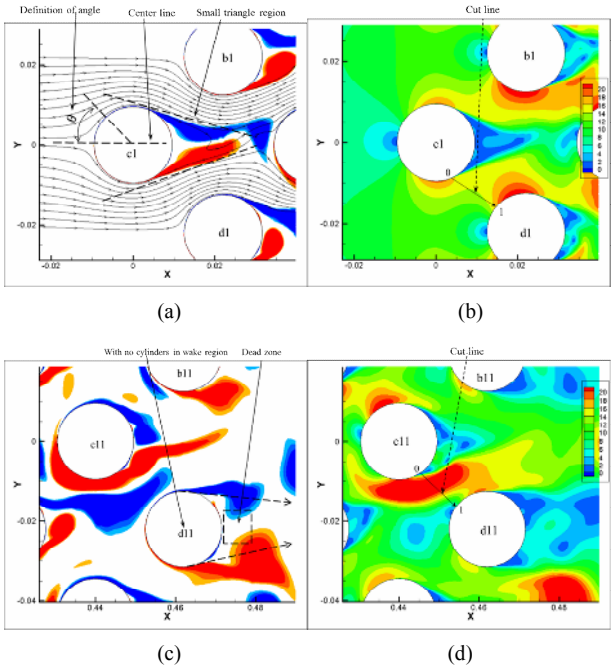

Fig. 7. Shedding vortices and velocity distribution overview of c1 and d11 at 0.6144 s: (a) Shedding vortices of c1; (b) velocity distribution of c1; (c) shedding vortices of c11 and d11; (d) velocity distribution between c11 and d11.

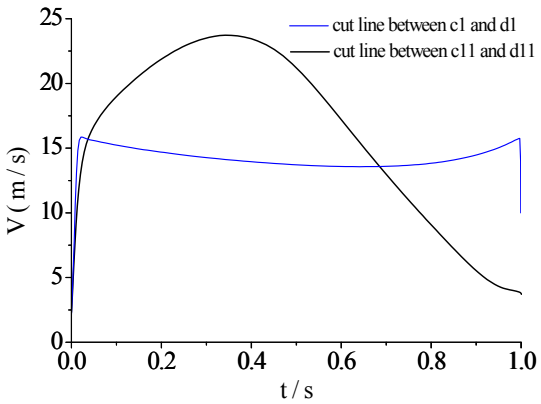

Fig. 8. Velocity distributions of the two cut lines.

Contours of velocity around c1 and c9 are depicted in Figs. 7(b) and (d), respectively. To quantitatively characterize the velocity distributions, a cut line is placed between c1 and b1 while another one is placed between c11 and d11. Distributions of velocity against time (unit, second) along the two cut lines are shown in Fig. 8. It is found that velocity is scarcely fluctuated along the cut line between c1 and b1 except at the begin and the end which are in boundary layers. On the contrary, velocity along the cut line between c11 and d11 varies widely, and a maximum of 23.4 m/s is achieved at a non-dimensional distance of 0.36. It is confirmed that the jet flow is induced by the interaction of strong anti-clockwise vortices and clockwise vortices.

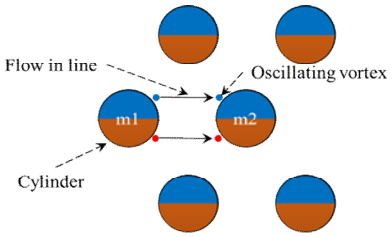

Fig. 9. Vortex pattern of *flow in line*.

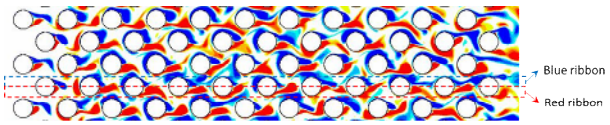

Fig. 10. Blue ribbon and red ribbon of shedding vortices.

3.2 Flow in line vortices

Each cylinder is a vortex generator, and the flow domain has been suffused with both abundant red vortices and abundant blue vortices passing the corresponding shear layers around a cylinder, which is named as *flow in line* in this paper as shown in Fig. 9. As a result, a blue ribbon and a red ribbon are formed as shown in Fig. 10. Take the blue ribbon for example, a blue vortex flow downstream to come up with some new blue shedding vortex, those vortices pair up with each other to pass downstream as a pair of co-rotating vortices till the end of the cylinder bundle. The generating, coalescing and dissipating of blue vortices finally construct the blue ribbon in the shear layers above a cylinder row. Practically, the *flow in line* below d5 is studied as shown in Fig. 11. It is shown that a red vortex is generated in the shear layer below d4 at 0.618 s while a new red vortex is generated in the shear layer below d5. The red vortex shed from d4 trickles, attracts and consolidates with the red vortex shed from d5, resulting in a stronger red vortex at 0.6189 s as shown in Fig. 11(b). Finally, the stronger red vortex flow downstream to capture a vortex pattern of *flow in line* as shown in Fig. 11(c).

3.3 Random shedding vortices

Feathers of the pattern of *flow in line* vortex have been discussed in Sec. 3.2.2. They are 'stable' for they happen all the time. However, some 'unstable' shedding vortices have been observed in the flow domain with random appearance which is difficult to predict. Those unstable vortices flow downstream not in one single ribbon but two or more. Here, unstable patterns of vortex shedding are classified as *cross in line*, *cross near line near*, *cross near line far* and *cross far line near*, respectively, as shown in Fig. 12, and we only take blue shedding vortex for example which is repeated by a red one. When a new blue vortex is formed in shear layer above m1, it may flow to the bottom of m2. In consideration of m1 and m2 are in the same line, the corresponding cross flow pattern is named as *cross in line*. Also, the blue vortex may reach the upper surface of m4. Because m4 is in a near line but far from

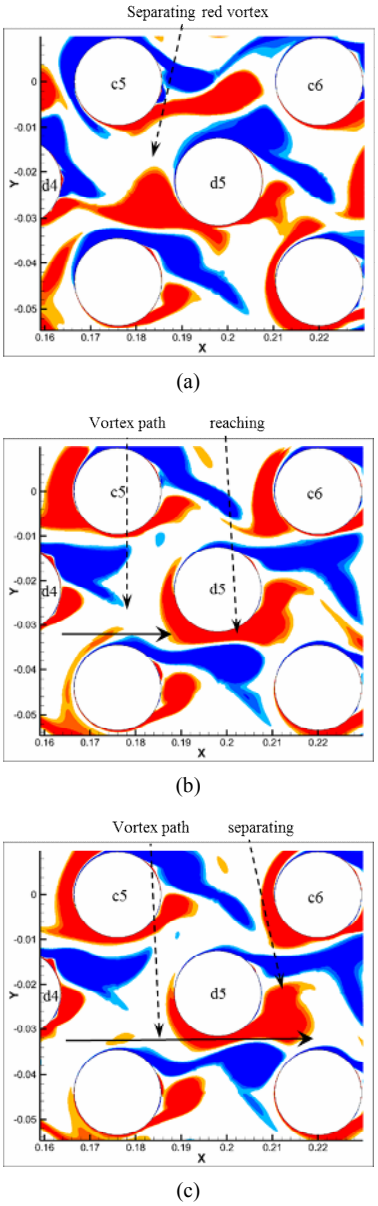

Fig. 11. Vortex pattern of *flow in line* of d5.

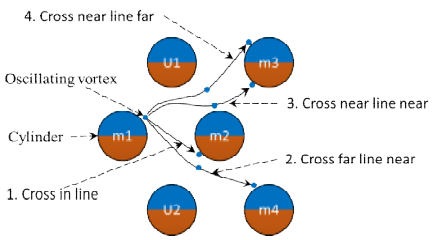

Fig. 12. Flow patterns with random shedding vortices.

the upper surface of m1, this cross-flow pattern is named as *cross far line near*. Similarly, the blue vortex may reach the upper surface of the bottom surface of m3, the corresponding patterns are named as *cross near line near*, *cross near line far*, respectively.

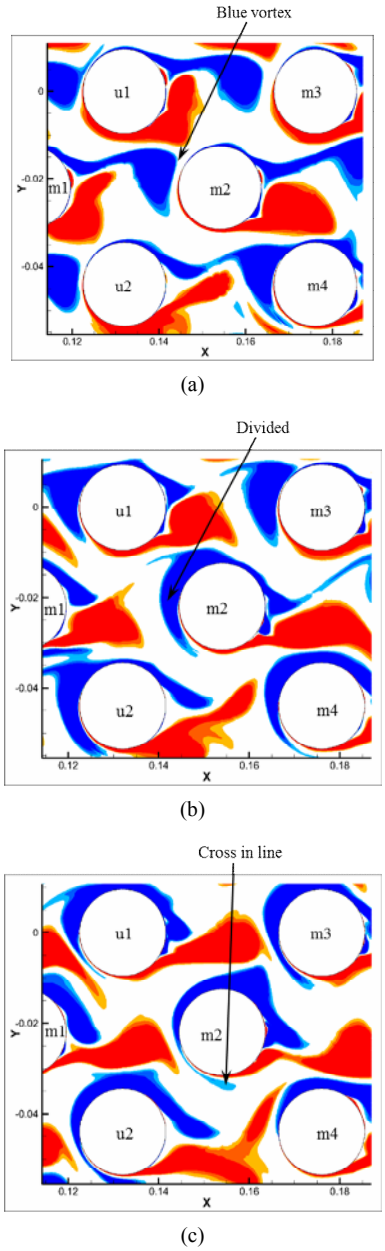

Fig. 13. Vortex pattern of *cross in line*.

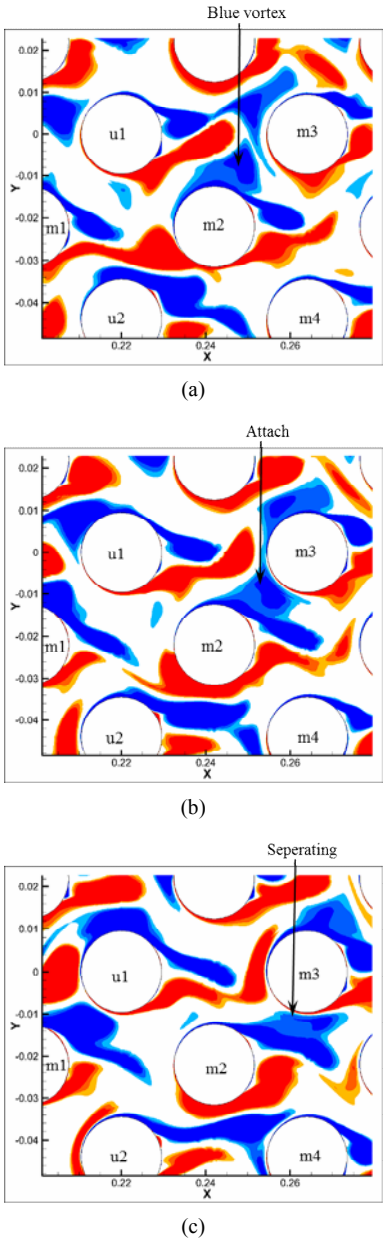

Fig. 14. Basic vortex pattern of *cross near line near*.

A series of cases are discussed to demonstrate the development of random shedding vortices. To be consistent with the arrangement of cylinders in Fig. 12, the cylinders are renamed as m1-m3, u1-u2. The vortex pattern of *cross in line* is the most common phenomena among the four unstable patterns evidenced by the shedding processes shown in Fig. 13. A deeper insight into the vortex pattern shows that a strong blue vortex is developed in the shear layer above the cylinder m1 followed by appearance of a strong red vortex in shear layer below u1. Till the meeting of the blue vortex and the red one ahead of m2, the red vortex will crush the blue one to deviate from the original flow direction. Once intensity of the red vortex is strong enough, the blue vortex may stride across the center line of m2 with part of it remained above m2, thereafter, the crossed part interacts with the bottom red vortices. However, the crossed blue vortex will be weakened and finally dissipated in the wake and the existence of vortex pattern of *cross in line* is usually short due to the opposite rotation.

The vortex pattern of *cross near line near* is evidenced by the shedding process depicted in Fig. 14. A blue vortex is generated by cylinder m1, the oscillating amplitude is becoming large as the vortex flow downstream to the shear layer above m2. Actually, vortices do not exist continuously but in a discrete form, and each vortex passes the corresponding ribbon one by one. Once no appearance of red vortex is found in the shear layer below m3, the blue vortex will reattach to the lower surface of m3 and move forward along the lower surface for a short distance, thus the vortex pattern of *cross near*

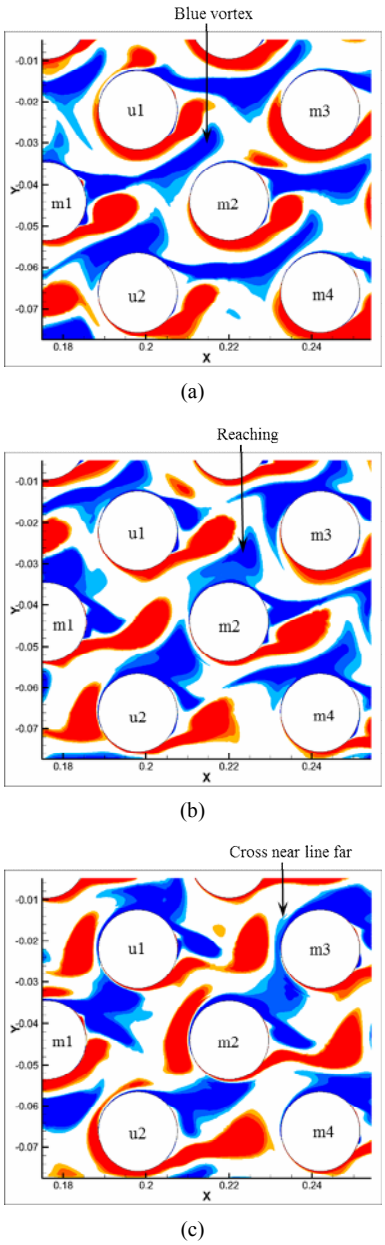

Fig. 15. Basic vortex pattern of *cross near line far.*

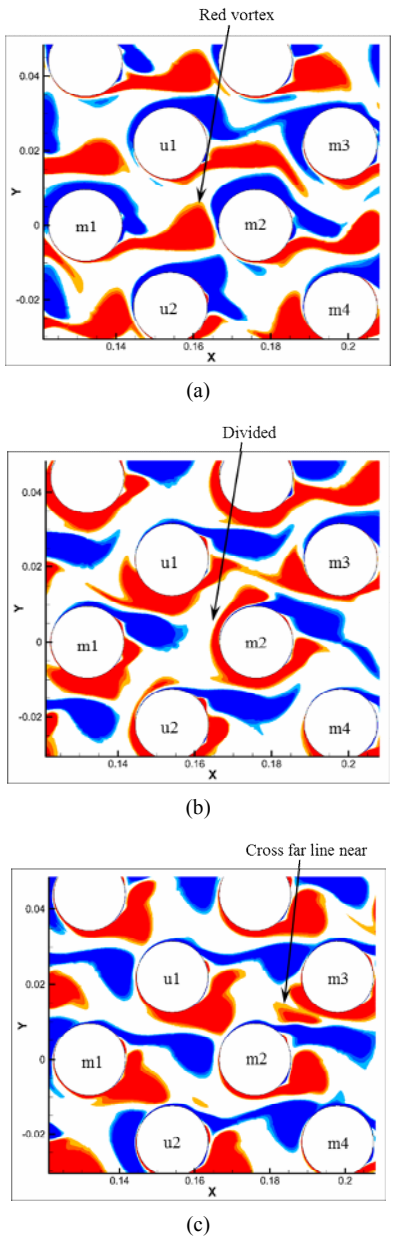

Fig. 16. Basic vortex pattern of *cross far line near.*

line near is established. However, once a red vortex flow downstream to the shear layer below m3, the reattachment of the blue vortex will be eliminated. Therefore, *cross near line near* exist only in a short time.

As mentioned previously, a blue vortex may reach the shear layer above m2 with a larger oscillating amplitude. If there is no red vortex reaching the leading edge of m3 combined with the assumption that the leading edge is surrounded by blue vortices which means that a phenomenon of *cross in line* occurred, the blue vortex coalesces with the one that adhering m3. In some particular situations, part of the blue vortex will stride across the center line of m3 and move toward the shear layer above m3 as shown in Fig. 15. The crossed blue vortex pairs up with those blue vortices above m3 and passes downstream as a large blue vortex. The result blue vortex flows freely and dissipates in the corresponding ribbon to form the phenomenon of *cross near line far*.

As discussed previously, a vortex may stride across the center line of m2. If the crossed red vortex is so strong that it cannot be dissipated in a short time, the divided vortex will flow into the shear layer above m2 and consolidate with a red upstream vortex to form a single stronger vortex as shown in Fig. 16. As a result, the stronger red vortex flow past the shear layer below m3 to confirm the vortex pattern of *cross far line near*. Rotating direction of the result red vortex is consistent with those in the red ribbon, the result vortex will flow freely and dissipate slowly in the corresponding ribbon like the vortex pattern of *cross near line far*.

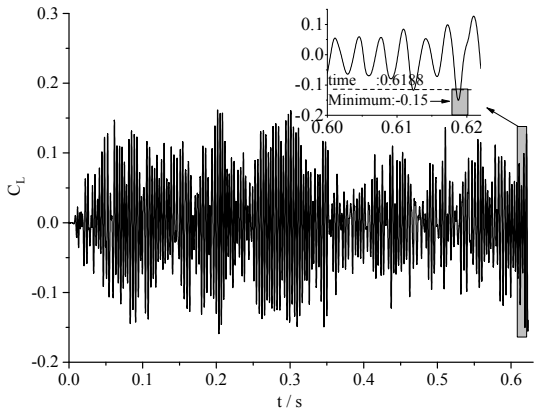

Fig. 17. Sudden increase of C_L of d5.

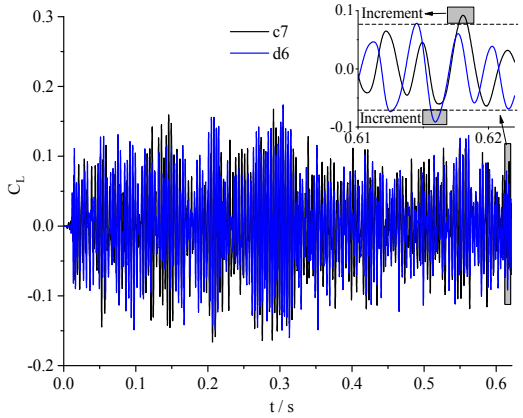

Fig. 18. Sudden increase of C_L of d6 and c7.

4. Influences of shedding vortices on lift performances

As discussed in Sec. 3, each cylinder is a vortex generator to produce lots of vortices in the flow domain. The key feature of interest for shedding vortices around cylinders is the periodic vortex shedding phenomenon and how it can lead to better understanding of influences on the unsteady performances. It has been confirmed that those *flow in line* vortices or random shedding vortices tremendously influence the lift performances of each cylinder leading to fluctuations of lifts with randomness. Here, 3 commonly influence effects have been studied which are *lift enhancement*, *lift pit* and *lift lag*.

The *lift enhancement* can be induced by both vortices of *flow in line* and random vortices evidenced by the history of the lift coefficients of d5 illustrated in Fig. 17. The C_L oscillate sinusoidally with an amplitude below 0.075 before 0.61 s. However, at time 0.6188 s, a pronounced maximum value of the C_L (absolute value) was observed to be 0.15 which is 2 times of 0.075 due to the vortex pattern of *flow in line*. This sudden increase of C_L is an irrefutable proof of the *lift enhancement* of *flow in line*. To reveal this mechanism, the shedding vortices around d5 has been studied shown in Fig. 11. As discussed in Sec. 3.2.2, the vortex pattern of *flow in line* occurs during 0.618 s to 0.6192 s. When a red vortex that shed from d4 reattached to d5 to confine a stronger red vortex, a high circulation of d5 achieves. These consistent observations indicate the lift enhancement of lift.

Random shedding vortices can also trigger the *lift enhancement* which is proofed by the *lift enhancements* of d6 and c7 presented in Fig. 18. It is shown that the lift coefficients of both d6 and c7 oscillate in a sinusoidal form with amplitudes below 0.075. However, the C_L of d6 attains a minimum value of -0.091 at 0.616 s while the C_L of d7 is pronounced to a maximum value of 0.092 at 0.618 s. This is confirmed by the corresponding evolutionary processes of vortices shed from d6 and c7. It is shown that a red vortex is divided into two parts at 0.6153 s as shown in Fig. 19(a). The smaller one goes through the lower shear layer while the stronger one flows across the center line, goes by the upper surface and reaches the shear layer above d6 at 0.6162 s fol-

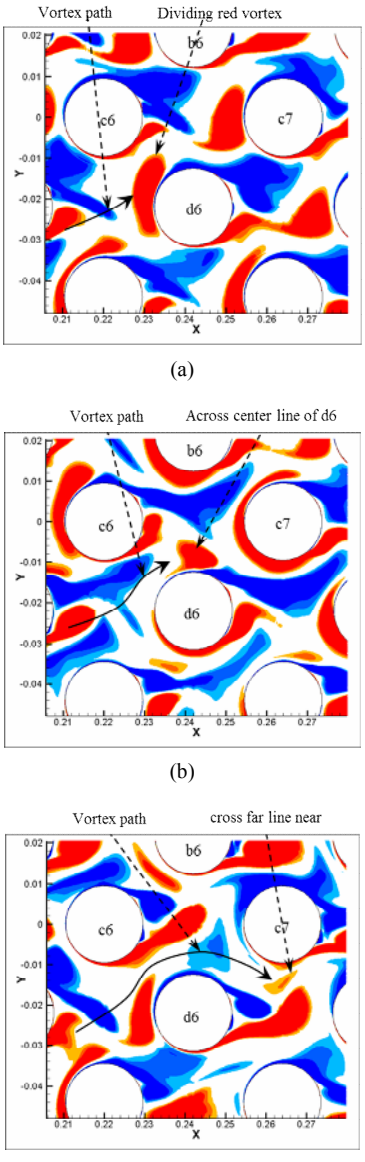

Fig. 19. Vortex of *cross far line near* of d6 and c7: (a) 0.6153 s; (b) 0.6162 s; (c) 0.618 s.

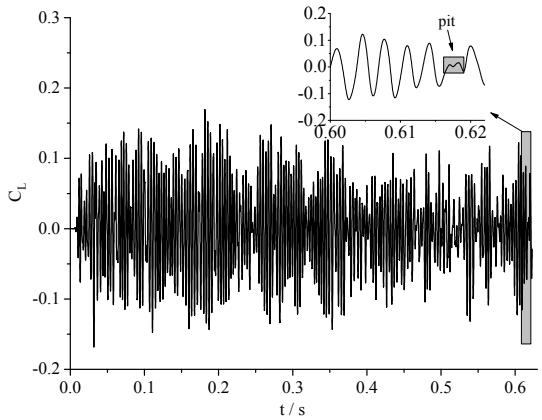

Fig. 20. Lift *pit* of x1.

lowed by generation of a red vortex with high intensity in the shear layer below d6. Thus, a high circulation of d6 achieves and a high lift is obtained. Thereafter, the divided red vortex with higher intensity above d6 will thrust the neighboring blue vortex up, as shown in Fig. 19(b). As a result, all the blue vortices above c7 go through the corresponding blue ribbon as shown in Fig. 19(c) leading to a lift enhancement of c7 by 22.6 % at time 0.618 s.

As the *lift pit*, Fig. 20 shows that the C_L of x1 decreases to a minimum value from 0.617 s till 0.6175 s at first, and then increases from 0.6175 s to 0.6183 s gradually, thereafter, the diminishing of C_L is more pronounced as time goes by, thus a pit appears in the figure. Similarly, vortices shed from x1 are investigated to study the flow mechanisms as shown in Fig. 21. It is shown that a blue vortex is separated in the shear layer above a1, then stride to the shear layer below x1, Figs. 21(a)-(c) details the vortex pattern of *cross near line near* as discussed in Sec. 3.3.3. The blue vortex cancels out the red vortex adhering x1 leading to a pronounced decrease of circulation around x1, thus the C_L has been reduced dramatically as soon as it reaches x1. However, the crossed blue vortex will go downstream rather than stick to the wall surface, The C_L will rehabilitate to the original situation after the *cross near line near*.

As the *lift lag*, Fig. 22 exhibits the time history of lift coefficients of c10 and c11. The C_L of c10 decreases until 0.6145 s, then keeps unchanged from 0.6145 s to 0.615 s followed by a decrease. Thus, a lag with 0.005 s has been observed. It is worth noticing that a similar *lift lag* also appears after 0.02 s in the C_L of c11. Fig. 23 shows evolutional processes of those vortex shedding to reveal the transfer phenomena. No vortex is separated from c9 until 0.6150 s leaving a white region without any vortex between c9 and c10, as shown in Fig. 23(a). During this time the lift of c10 keeps nearly unchanged. The red vortex then sheds downstream, consolidates and attracts with vortices around c10 to put off the corresponding vortex shedding of c10. As a result, there is no vortex reaching the leading of c11 until 0.6171 s and the lift of c11 keeps nearly unchanged during this time gap. Therefore, the *lift lag* of c10 has been transported to c11.

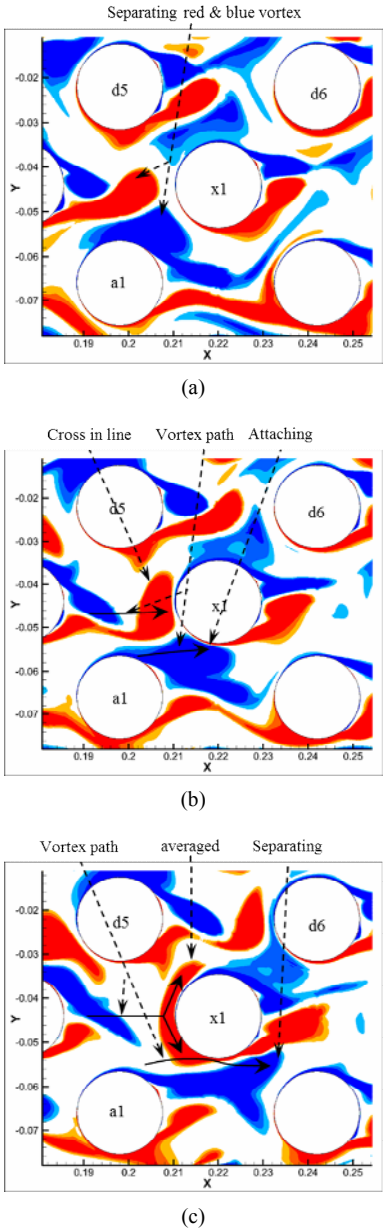

Fig. 21. Vortex of cross *near line near* and *cross in line* of x1: (a) 0.6165 s; (b) 0.6171 s; (c) 0.6177 s.

5. Conclusions

In this study, numerical simulations have been carried out to study the shedding vortices in cross flow with 253 cylinders. Statistics and randomness are found to be the two main characteristics of the shedding vortices.

As the Statistics, blue vortices are generated and shed in shear layers above a cylinder while red vortices are generated and shed below each cylinder. These two kinds of vortices flow downstream in a vortex pattern of *flow in line*, which resulting in the blue and the red ribbon. Above all, the vortex

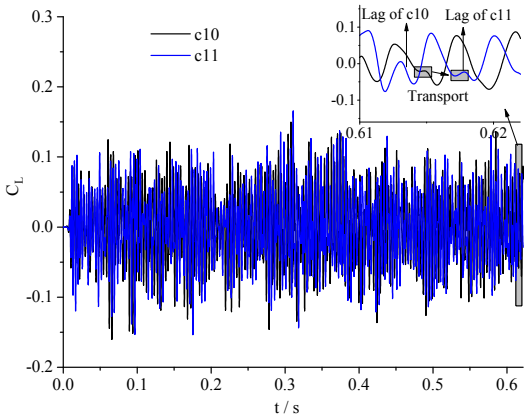

Fig. 22. Lift *lag* of C_L of c10 and c11.

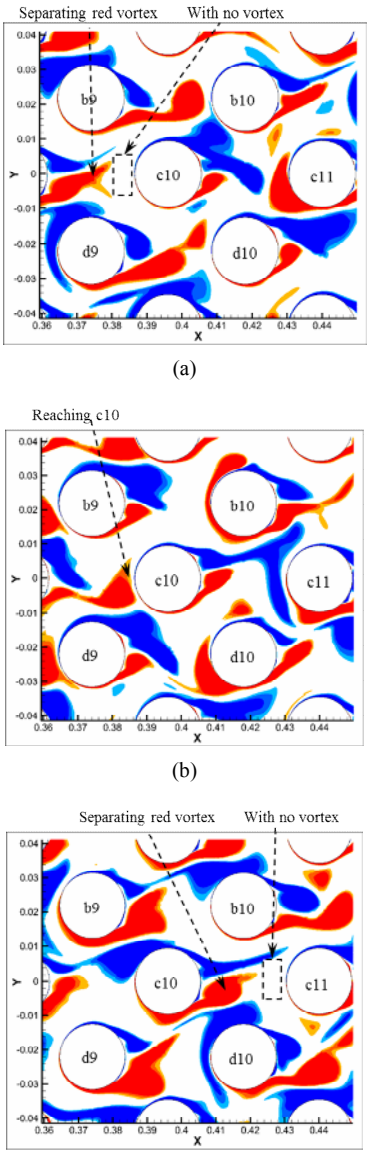

(a)

(b)

(c)

Fig. 23. Vortex of c10 and c11: (a) 0.6138 s; (b) 0.6150 s; (c) 0.6171 s.

pattern *flow in line* is 'stable'.

However, some 'unstable' vortices patterns may appear occasionally. As the random shedding vortices, four basic random vortex patterns have been summarized as *cross in line*, *cross near line near*, *cross near line far* and *cross far line near* in this paper. Those unstable vortices appear randomly and it is quite difficult to predict. Also, random vortex pattern may not appear solely, two or more vortex patterns may appear at the same time. Each strong shedding vortex induces a high circulation, therefore the influences of unstable vortices on the lift coefficients may be so great that cannot be neglected. Here, three commonly influence patterns of random vortices on the lift coefficients have been summarized as *lift enhancement*, *lift pit* and *lift lag*. The C_L can be increased by 2 times due to the shedding vortices as depicted in the *lift enhancement*. The random shedding vortices may also induce a lift pit or a lift lag which will change the amplitudes and frequencies of lifts.

Acknowledgments

The authors would like to thank the referees for their good and valuable suggestions which improved this paper greatly. The work is supported by National Natural Science Foundation of China (51705459) and China Postdoctoral Science Foundation.

Nomenclature

ρ	: The density
V	: The magnitude of velocity
t	: The time
μ	: The coefficient of dynamic viscosity
p	: The pressure
ω_z	: The vorticity in z direction
L	: The lift force
C_L	: The lift coefficient

References

[1] J. Baek, A panel cointegration analysis of CO_2 emissions, nuclear energy and income in major nuclear generating countries, *Applied Energy*, 145 (2015) 133-138.

[2] M. Al-Zareer, I. Dincer and M. A. Rosen, Performance analysis of a supercritical water-cooled nuclear reactor integrated with a combined cycle, a Cu-Cl thermochemical cycle and a hydrogen compression system, *Applied Energy*, 195 (2017) 646-658.

[3] R. Pattupara and R. Kannan, Alternative low-carbon electricity pathways in Switzerland and it's neighbouring countries under a nuclear phase-out scenario, *Applied Energy*, 172 (2016).

[4] R. Govardhan and C. H. K. Williamson, Modes of vortex formation and frequency response of a freely vibrating cylinder, *Journal of Fluid Mechanics*, 420 (2000) 85-130.

[5] N. Maïzi and E. Assoumou, Future prospects for nuclear

power in France, *Applied Energy,* 136 (2014) 849-859.
[6] L. Tang, L. Yu and K. He, A novel data-characteristic-driven modeling methodology for nuclear energy consumption forecasting, *Applied Energy*, 128 (2014) 1-14.
[7] S. Kosai and H. Unesaki, Quantitative analysis on the impact of nuclear energy supply disruption on electricity supply security, *Applied Energy*, 208 (2017) 1198-1207.
[8] L.-C. Hsu, C.-L. Chen and J.-Z. Ye, A study of flow patterns for staggered cylinders at low Reynolds number by spectral element method, *Journal of Mechanical Science and Technology*, 31 (2017) 2765-2780.
[9] D. Tang, S. Bao, L. Luo, H. Zhu and H. Cui, A CFD/CSD coupled method with high order and its applications in flow induced vibrations of tube arrays in cross flow, *Annals of Nuclear Energy*, 130 (2019) 347-356.
[10] M. Coutanceau and J. R. Defaye, Circular cylinder wake configurations: A flow visualization survey, *Applied Mechanics Reviews*, 44 (5) (1991) 255-305.
[11] P. W. Bearman and M. M. Zdravkovich, Flow around a circular cylinder near a plane boundary, *Journal of Fluid Mechanics*, 89 (1) (1978) 639-650.
[12] G. Buresti and A. Lanciotti, Mean and fluctuating forces on a circular cylinder in cross-flow near a plane surface, *Journal of Wind Engineering And Industrial Aerodynamics*, 41 (1992) 1-3.
[13] T. Nishino, G. T. Roberts and X. Zhang, Vortex shedding from a circular cylinder near a moving ground, *Physics of Fluids*, 19 (2) (2007) 025103.
[14] Q. Wang, M. Li and S. Xu, Experimental study on vortex induced vibration (VIV) of a wide-D-section cylinder in a cross flow, *Theoretical and Applied Mechanics Letters*, 5 (1) (2015) 39-44.
[15] Bundesamt für Energie, *Schweizerische Elektrizitätsstatistik*, Swiss Federal Statistical Office, Bern (2014).
[16] D. Sumner, M. D. Richards and O. O. Akosile, Two staggered circular cylinders of equal diameter in cross-flow, *Journal of Fluids and Structures*, 20 (2) (2005) 255-276.
[17] S. J. Price, M. P. Paidoussis and S. Krishnamoorthy, Cross-flow past a pair of nearly in-line cylinders with the upstream cylinder subjected to a transverse harmonic oscillation, *Journal of Fluids and Structures*, 23 (1) (2007) 39-57.
[18] M. M. Zdravkovich, The effects of interference between circular cylinders in cross flow, *Journal of Fluids and Structures*, 1 (2) (1987) 239-261.
[19] G. R. S. Assi, N. Srinil, C. M. Freire and I. Korkischko, Experimental investigation of flow-induced vibration interference between two cylinders, *Journal of Fluids and Structures*, 22 (6) (2006) 819-827.
[20] X. Li, X. Wu and S. He, Numerical investigation of the turbulent cross flow and heat transfer in a wall bounded tube bundle, *International Journal of Numerical Methods for Heat & Fluid Flow*, 75 (1) (2014) 127-139.
[21] M. M. Zdravkovich, *Flow Around Circular Cylinders*, Oxford University Press, New York (2003).
[22] D. S. Weavera and M. Elkashlana, On the number of tube rows required to study cross-flow induced vibrations in tube banks, *Journal of Sound and Vibration*, 75 (2) (1981) 265-273.
[23] R. Duan and S. Jiang, Numerical investigation of gas flow distribution and thermal mixing in helically coiled tube bundle, *Journal of Nuclear Science And Technology*, 45 (7) (2008) 704-711.
[24] B. de Pedro, J. Parrondo, C. Meskell and J. F. Oro, CFD modelling of the cross-flow through normal triangular tube arrays with one tube undergoing forced vibrations or fluidelastic instability, *Journal of Fluids and Structures*, 64 (2016) 67-86.
[25] A. G. Abramov, A. M. Levchenya, E. M. Smirnov and P. E. Smirnov, Numerical simulation of liquid metal turbulent heat transfer from an inline tube bundle in cross-flow, *St. Petersburg Polytechnical University Journal: Physics and Mathematics*, 4 (2015) 356-363.
[26] A. Zanotti, R. Nilifard, G. Gibertini, A. Guardone and G. Quaranta, Assessment of 2D/3D numerical modeling for deep dynamic stall experiments, *Journal of Fluids and Structures*, 51 (2014) 97-115.
[27] S. Wang, D. B. Ingham, L. Ma, M. Pourkashanian and Z. Tao, Turbulence modeling of deep dynamic stall at relatively low Reynolds number, *Journal of Fluids and Structures*, 33 (2012) 191-209.
[28] A. Roshko, On the wake and drag of bluff bodies on the wake and drag of bluff bodies, *Jour Aeronautical Sci.*, 22 (2) (1955) 124-132.
[29] A. Roshko, Experiments on the flow past a circular cylinder at very high reynolds number, *Journal of Fluid Mechanics*, 10 (3) (1960) 345-356.
[30] J. H. Gerrard, The mechanics of the formation region of vortices behind bluff bodies, *Journal of Fluid Mechanics*, 25 (2) (1966) 401-413.
[31] A. S. Grove, F. H. Shair, E. E. Petersen and A. Acrivos, An experimental investigation of the steady separated flow past a circular cylinder, *Journal of Fluid Mechanics*, 19 (1964) 60-80.
[32] S. S. Paul, S. J. Ormiston and M. F. Tachie, Experimental and numerical investigation of turbulent cross-flow in a staggered tube bundle, *International Journal of Heat & Fluid Flow*, 29 (2) (2008) 387-414.
[33] J. K. Ostanek and K. A. Thole, Wake development in staggered short cylinder arrays within a channel, *Experiments in Fluids*, 53 (3) (2012) 673-697.
[34] C. K. Mangrulkar, A. S. Dhoble, S. G. Chakrabarty and U. S. Wankhede, Experimental and CFD prediction of heat transfer and friction factor characteristics in cross flow tube bank with integral splitter plate, *International Journal of Heat & Mass Transfer*, 104 (2017) 964-978.
[35] D. Tang, S. Bao, L. Luo, J. Mao, B. Lv and H. Guo, Study on the aeroelastic responses of a wind turbine using a coupled multibody-FVW method, *Energy*, 141 (2017) 2300-2313.
[36] TEMA, *Standards of the Tubular Exchanger Manufactur-*

ers Association, Eighth edition (1999).
[37] GB151-99, *Tubular Heat Exchangers*, Standards Press of China (1999).
[38] M. Xu and M. Wei, Using adjoint approach to study flapping wings, *Journal of Fluid Mechanics*, 799 (2016) 56-99.
[39] M. Xu, M. Wei, T. Yang and Y. S. Lee, An embedded boundary approach for the simulation of a flexible flapping wing at different density ratio, *European Journal of Mechanics (B/Fluids)*, 55 (2016) 146-156.
[40] D. Tang, Z. Fan, M. Lei, B. Lv, L. Yu and H. Cui, A combined airfoil with secondary feather inspired by the golden eagle and its influences on the aerodynamics, *Chinese Physics B*, 28 (3) (2019) 034702.
[41] C. Moulinec, M. J. B. M. Pourquie, B. J. Boersma, T. Buchal and F. T. M. Nieuwstadt, Direct numerical simulation on a Cartesian mesh of the flow through a tube bundle, *International Journal of Computational Fluid Dynamics*, 18 (1) (2004) 1-14.
[42] H. Jiang, L. Cheng, S. Draper and H. An, Prediction of the secondary wake instability of a circular cylinder with direct numerical simulation, *Computers & Fluids*, 149 (2017) 172-180.
[43] F. Shang, L. Hu, X. Sun, Q. Wang and A. Palacios, Flame downwash length evolution of non-premixed gaseous fuel jets in cross-flow: Experiments and a new correlation, *Applied Energy*, 198 (2017) 99-107.
[44] V. Shinde, T. Marcel, Y. Hoarau, T. Deloze and G. Harran, Numerical simulation of the fluid-structure interaction in a tube array under cross flow at moderate and high Reynolds number, *Journal of Fluids and Structures*, 47 (2014) 99-113.
[45] Y. Wang, A. Shukla and S. Liu, A state of art review on methodologies for heat transfer and energy flow characteristics of the active building envelopes, *Renewable & Sustainable Energy Reviews*, 78 (2017) 1102-1116.
[46] F. R. Menter, Two-equation eddy-viscosity turbulence models for engineering application, *AIAA. Journal*, 32 (8) (1994) 1598-1605.
[47] I.-C. Chu, H. J. Chung and S. Lee, Flow-induced vibration of nuclear steam generator U-tubes in two-phase flow, *Nuclear Engineering and Design,* 241 (5) (2011) 1508-1515.
[48] J. Duan, J. Gong, H. Yao, T. Deng and J. Zhou, Numerical modeling for stratified gas-liquid flow and heat transfer in pipeline, *Applied Energy*, 115 (2014) 83-94.
[49] E. Achenbach, Distribution of local pressure and skin friction around a circular cylinder in cross-flow up to Re=5×106, *Journal of Fluid Mechanics*, 34 (4) (1968) 625-639.
[50] D. Tang, S. Bao, M. Xu, L. Luo, B. Lv, L. Yu and H. Cui, On the number of tubes required to study oscillating vortices and frequency spectrums of tube arrays in cross flow, *Annals of Nuclear Energy*, 124 (2019) 198-210.
[51] A. Surendran, M. A. Heckl, L. Peerlings, S. Boij, H. Boden and A. Hirschberg, Aeroacoustic response of an array of tubes with and without bias-flow, *Journal of Sound and Vibration*, 434 (2018) 1-16.
[52] Q. M. Al-Mdallal and F. M. Mahfouz, Heat transfer from a heated non-rotating cylinder performing circular motion in a uniform stream, *International Journal of Heat & Mass Transfer*, 112 (2017) 147-157.

Di Tang received his Ph.D. degree in Nanjing University of Aeronautics and Astronautics, China. Currently, he is a researcher at Zhejiang University of Technology, China. His research interests include the fluid induced vibrations, vortex flow and bioinspired materials.